Sensors & Actuators: A. Physical 380 (2024) 116029

Contents lists available at ScienceDirect

Sensors and Actuators: A. Physical

journal homepage: www.journals.elsevier.com/sensors-and-actuators-a-physical

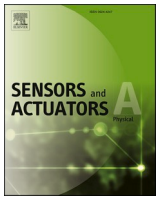

Multi-resonance-cavity hydrophone for underwater acoustic data transmission

Zan Li [a], Tian Yang [a], Jian Li [a], Jinyu Ma [a,*], Xinjing Huang [a,b,**]

[a] State Key Laboratory of Precision Measurement Technology, Tianjin University, Tianjin 300072, China
[b] Guangxi Key Laboratory of Automatic Detecting Technology and Instruments, Guilin University of Electronic Technology, Guilin, Guangxi, China

ARTICLE INFO

Keywords:
Hydrophone
Resonant air cavity
Underwater data transmission

ABSTRACT

Transmitting data from the seabed platform to relay buoys using wireless transmission techniques is becoming the main approach for seabed platform data retrieval, and data transmission via underwater acoustic waves offers certain advantages compared to that via underwater optical or electromagnetic waves. Hydrophones play a crucial role in underwater acoustic transmission, and low-cost, miniaturized, high-sensitive hydrophones based on resonance cavity meet the demands of seabed platform data retrieval scenarios. This paper proposes a multi-resonance-cavity hydrophone for underwater acoustic data transmission. The acoustic resonance characteristics of the cavity is studied through theoretical analysis and simulations. An eight-layer spherical cavity hydrophone is designed and fabricated, and the acoustic sensing characteristics and performances of the hydrophone are simulated and tested. Finally, underwater acoustic data receiving tests using the proposed hydrophone are conducted in a lake, demonstrating the hydrophone's ability to accurately receive acoustic data at the baud rate of 145.45 bps with no error.

1. Introduction

The seabed platform serves as a seabed observation device designed for the prolonged, continuous, fixed-point, and automatic monitoring of oceanographic information within specific sea areas. It is capable of monitoring hydrological, physical, chemical, biological, and geological parameters around the clock, and completing the acquisition, storage, and transmission of the monitoring data [1,2]. Seabed platform data retrieval technology is of great significance for constructing an intelligent three-dimensional perception system for the marine environment. Three types of methods are employed for seabed platform data retrieval: whole device retrieval [3,4], data pod retrieval [5], and data retrieval via relay buoys, whereas the first two methods face high costs, long cycles, and risks of data loss. For the third method, the seabed platform needs to transmit data to relay buoys using either wired or wireless techniques. The wired transmission techniques [6–9] typically utilize optical fiber cables to transmit data, offering benefits such as good data accuracy, high transmission rate and low latency. Despite these advantages, these techniques are susceptible to water depth and terrain, and the deployment and maintenance of the devices are difficult and expensive, thus suitable for the platforms near the coast. On the other hand, the wireless transmission techniques are not restricted by cables, offering benefits such as easy deployment, high flexibility, and longer transmission distances, and are gradually becoming the commonly used techniques.

Underwater wireless transmission techniques include optical, electromagnetic, and acoustic transmission. Underwater optical transmission [10,11] commonly utilizes green light (450–550 nm) or red light (625–740 nm) as the carrier wave, offering low latency and transmission rates of up to Gbps. However, absorption, reflection, and scattering of optical waves by seawater, marine organisms and small suspended particles lead to rapid attenuation. Additionally, due to its strong directivity, optical transmission requires precise alignment and unobstructed line-of-sight between transmitters and receivers, limiting the application of optical transmission. Underwater electromagnetic transmission [12,13] utilizes various electromagnetic waves (e.g., radio, microwave) as the carrier wave, exhibiting certain penetration capabilities in seawater and transmission rates of up to Mbps. Electromagnetic transmission is impervious to noise interference and has no adverse effects on marine organisms, but it requires large-sized antennas and

* Corresponding author.
** Corresponding author at: State Key Laboratory of Precision Measurement Technology, Tianjin University, Tianjin 300072, China.
E-mail addresses: jinyu.ma@tju.edu.cn (J. Ma), huangxinjing@tju.edu.cn (X. Huang).

https://doi.org/10.1016/j.sna.2024.116029
Received 8 July 2024; Received in revised form 17 September 2024; Accepted 3 November 2024

high power, resulting in high costs. Underwater acoustic transmission [14,15] utilizes acoustic waves as the carrier wave. Different frequency bands of acoustic waves are employed according to the transmission distance, with low-frequency, high-power waves capable of propagating for thousands of kilometers. Acoustic waves experience significantly lower attenuation underwater compared to optical and electromagnetic waves, and exhibit excellent diffraction capabilities, enabling stable transmission over long distances in various complex underwater environments. Furthermore, underwater acoustic transmission systems are characterized by simple equipment and high energy efficiency, which is beneficial for resource-limited seabed platforms and relay buoys, extending their lifespans and reducing maintenance costs. However, challenges persist in the use of acoustic transmission for seabed data retrieval. Researchers primarily focus on signal modulation and demodulation, communication protocols, network architectures, and transmission channel modeling [16–19], with relatively less emphasis on the research of acoustic sensors. Efforts should be made to control the cost and power consumption and enhance the accuracy in the acoustic transmission between seabed platforms and relay buoys.

The acoustic sensors at the front end of the buoys play a crucial role in the acoustic transmission between seabed platforms and relay buoys. The most used underwater acoustic sensor is the hydrophone, which includes various types such as piezoelectric ceramic hydrophones, polyvinylidene difluoride hydrophones, piezoelectric composite material hydrophones, and fiber optic hydrophones [20–24]. Piezoelectric hydrophones have mature technology and have been widely applied in various underwater acoustic detection fields. Fiber-optic hydrophones, with their high sensitivity, large dynamic range, resistance to electromagnetic interference and multiplexing capabilities, have attracted increasing attention in recent years for applications such as monitoring low-frequency signals, including those from earthquakes [25–28]. However, both commercial piezoelectric and fiber-optic hydrophone products are generally expensive, with complex manufacturing processes. In the application scenarios of seabed platform acoustic transmission, there is a need for low-cost, omnidirectional, and miniaturized hydrophones. Compared to the conventional hydrophones, hydrophones based on the principle of acoustic resonance cavity offer excellent cost control, simple manufacturing processes, and higher sensitivity advantages, meeting the demands of seabed platform data retrieval scenarios. Huang proposed a high-sensitivity, low-cost hydrophone based on acoustic resonance air cavity [29]. This hydrophone seals a small microphone at the center of a spherical air cavity and utilizes the acoustic resonance of the cavity to enhance sensitivity at the resonant frequency, enabling the detection of sound transmitted from all directions to the air cavity. The acoustic resonance cavity has also been used to design a spherical detector for pipeline leak detection, enabling high-sensitivity detection of broadband leak signals within pipelines [30].

This paper addresses the wireless data retrieval needs of seabed platforms and proposes a hydrophone with multiple resonance air cavities for underwater acoustic data transmission. The acoustic sensing characteristics of the spherical cavity and its stacked structures are investigated through theoretical analysis and finite element simulations. Laboratory tests are conducted in a water tank to validate the performance of the multi-resonance-cavity hydrophone for capturing single-frequency pulses. Customized data modulation and demodulation methods are proposed for this hydrophone, and a system is set up to test its data parsing performance. Finally, lake tests on acoustic data transmission are carried out to evaluate the transmission speed and accuracy with the proposed hydrophone.

2. Design of the hydrophone

2.1. Theoretical analysis of spherical cavity resonance modes

For the air cavity within the rigid spherical shell, due to the reflection of the shell, the acoustic waves inside the air cavity exist in the form of standing waves, thus enabling a rigorous description and analysis using the normal mode theory. The normal modes represent the standing wave modes, and the normal frequencies correspond to the resonance frequencies of the cavity. Denote the radius of the air cavity as a, and the sound speed as c_0. In the r-θ-ϕ spherical coordinate system, the equations satisfied by the normal modes ψ_λ and the normal frequencies ω_λ are [31]:

$$\left[\frac{1}{r^2}\frac{\partial}{\partial r}\left(r^2\frac{\partial}{\partial r}\right)+\frac{1}{r^2\sin\theta}\frac{\partial}{\partial\theta}\left(\sin\theta\frac{\partial}{\partial\theta}\right)+\frac{1}{r^2\sin^2\theta}\frac{\partial^2}{\partial\phi^2}\right]\psi_\lambda+\left(\frac{\omega_\lambda}{c_0}\right)^2\psi_\lambda=0\# \tag{1}$$

with the boundary condition:

$$\left.\frac{\partial\psi_\lambda}{\partial r}\right|_{r=a}=0\# \tag{2}$$

The solution of (1) can be expressed as:

$$\psi(r,\theta,\varphi,\omega_\lambda)=\left[A_l\mathrm{j}_l\left(\frac{\omega_\lambda}{c_0}r\right)+B_l\mathrm{n}_l\left(\frac{\omega_\lambda}{c_0}r\right)\right]\mathrm{Y}_l^m(\theta,\varphi)\# \tag{3}$$

where j_l and n_l are Bessel functions of the first and the second types, and $\mathrm{Y}_l^m(\theta,\varphi)$ is the spherical harmonics, l, m are integers, $l\geq 0$, $-l\leq m\leq l$. When $r=0$, $\mathrm{n}_l(0)\to\infty$, so that $B_l\equiv 0$. Therefore, obtained from (2), the normal frequencies satisfy:

$$\mathrm{j}_l'\left(\frac{\omega_\lambda}{c_0}a\right)=0\# \tag{4}$$

Let x_{ql} be the q^{th} root of the equation $\mathrm{j}_l'(x)=0$, then the normal frequency $\omega_\lambda=\omega_{nl}$ can be expressed as:

$$\omega_{nl}=\frac{c_0x_{nl}}{a}\quad(n=0,\quad 1,\quad 2,\ldots;l=0,\quad 1,\quad 2,\ldots)\# \tag{5}$$

Therefore, the normal frequency is determined by the spherical Bessel function equation, and the normal frequency of each mode is inversely proportional to the radius of the air cavity. Specific resonance frequencies can be obtained by varying the radius of the spherical cavity.

2.2. Simulation validation of spherical cavity resonance modes

A three-dimensional model of the air cavity was established, and finite element simulations were conducted on the spherical cavity resonance modes in pressure acoustics field. Due to the similarity in resonance modes among cavities of different radii, simulations were performed using the cavity with a radius of 20 mm as an example. The first three resonance frequencies of this cavity are f_1=5685.1 Hz, f_2=9127.7 Hz, and f_3=12272 Hz. The normalized absolute pressure distributions and directivity patterns at these three resonance frequencies are illustrated in Fig. 1(a)-(f).

At the first resonance frequency, the absolute pressure is symmetrically distributed about the equatorial plane, with the highest absolute pressure occurring at the two poles and decreasing towards the equatorial plane. The absolute pressure near the center of the cavity approaches 0 Pa. This bidirectional mode exhibits an 8-shaped directivity, with the maximum sensitivity directed towards the sound source. At the second resonance frequency, the absolute pressure reaches the maximum at the four poles and decreases when moving away from the poles. Similar to the first mode, the absolute pressure near the center of the cavity also approaches 0 Pa. This mode exhibits a four-leaf clover-shaped directivity. At the third resonance frequency, the absolute pressure reaches the maximum at the center of the sphere and decreases when moving outward from the center. This mode is omnidirectional, with each point at the same radius of the cavity exhibiting equal sensitivity to sound sources from all directions. By comparing these three modes, it is evident that at the third resonant frequency, the center of the cavity exhibits high sensitivity and omnidirectionality, making it

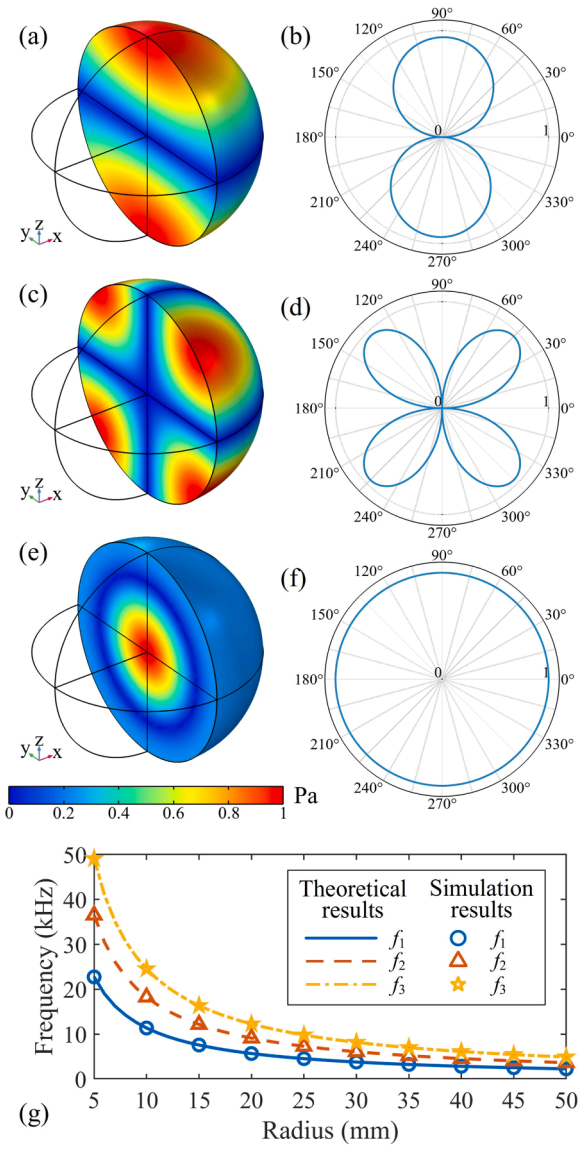

Fig. 1. Simulation validation of spherical cavity resonance modes: (a)-(f) normalized absolute pressure distribution and directivity patterns at the first three resonance frequencies; (g) the relationship between the theoretical and simulated resonance frequencies and the radius of the spherical cavity.

capable of receiving signals from any direction.

A parametric sweep on the radius of the spherical cavity was conducted, ranging from 5 mm to 50 mm with a step of 5 mm. The simulation results of the first three resonance frequencies of each spherical cavity, along with their theoretical values, are plotted in Fig. 1(g). From the figure, it can be observed that the first three resonance frequencies f_1, f_2, f_3 exhibit an inverse proportional relationship with the radius of the spherical cavity, decreasing as the radius increases, consistent with (5). The third resonance frequencies of the various spherical cavities are separate and do not interfere with each other, thus enabling the serial connection of multiple spherical cavities and the simultaneous utilization of their third resonance modes for acoustic sensing.

2.3. Design and simulation of the multi-resonance-cavity hydrophone

Inspired by the previous study of rigid shell resonance air cavities, a multi-resonance-cavity hydrophone is proposed, which is based on the omnidirectionality of the third-order resonance mode of the spherical cavity and the fact that spherical cavities with different radii have different resonance frequencies. Multiple spherical cavities with different radii are stacked, and acoustic sensors are placed at the center of each cavity to capture acoustic signals. Since the acoustic pressure at the center is significant at the third-order resonance frequency and is minimal at the first, second and other non-resonant frequencies, the sensors are possible to accurately capture signals at the third-order resonance frequency without interference from the other frequencies. All sensors in the cavities synchronously capture signals at their third-order resonance frequencies, thus enabling the hydrophone to capture multi-frequency signals. Consequently, a stacked spherical cavity structure composed of two/four/eight cavities is designed, as shown in Fig. 2(a). The presence or absence of a specific frequency component in the multi-frequency signal represents data as "1" or "0". Each cavity receives one bit of data, theoretically enabling the receiving of two/four/eight bits of data.

The three-dimensional model of the eight-layer spherical cavity hydrophone was constructed, and its frequency response was simulated to study the influence of the shell and the sensor circuit board on the resonance frequency of the cavity. The simulation model is shown in Fig. 2(b). The hydrophone is placed at the center of a rectangular water area, and acoustic waves are incident from the right boundary. The hydrophone is composed of eight hollow spheres made of photosensitive resin, with the cavities filled with air. Several cubes of 4 mm long and 1 mm wide traverse the cavities, functioning as the sensor circuit board. The eight spheres are numbered from 1 to 8 in order of size, with cavity radii of 10 mm, 12.5 mm, 15 mm, 17.5 mm, 20 mm, 22.5 mm, 25 mm, and 27.5 mm, and the shell thickness of 2 mm.

The frequency sweep range was 7 kHz to 26 kHz, with a step of 50 Hz. Taking the center of each sphere as the measurement point, the frequency response curves of each point are plotted in Fig. 2(c), where the resonance peaks corresponding to the third-order resonance frequencies of each cavity are marked with colored arrows. From the

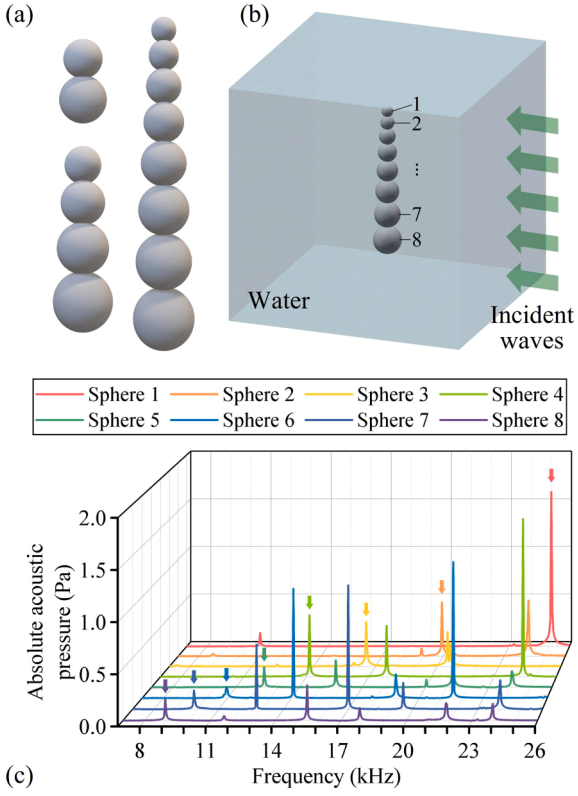

Fig. 2. Design and simulation of the multi-resonance-cavity hydrophone: (a) two/four/eight-layer spherical cavity structure; (b) simulation model of the hydrophone; (c) frequency response curves of each channel.

results, it can be observed that the center of each cavity exhibits prominent absolute acoustic pressure at resonance frequencies, while the pressure is relatively low at other frequencies; the presence of the shell and sensor circuit board has minimal effect on the third-order resonance mode of the cavity. The unmarked resonance peaks originate from higher-order resonance modes, but they do not affect the reception of signals at the third-order resonance frequencies. Instead, these higher-order modes can be utilized to realize transmission of more bits theoretically.

Another mechanical finite element simulation was conducted to assess the hydrostatic pressure resistance of the hydrophone shell. The simulation model is shown in Fig. 3(a). A boundary load was applied to the external wall of the photosensitive resin shell, with the pressure ranging from 1 MPa to 10 MPa, corresponding to water depths from about 100–1000 m. The average von Mises stresses on the internal wall of each cavity under various pressures are illustrated in Fig. 3(b). It can be inferred that a 2 mm thick photosensitive resin shell (yield strength 56.8 MPa) can theoretically resist the hydrostatic pressure of about 7 MPa, and a metal shell (yield strength generally more than 100 MPa) of more than 10 MPa. Moreover, increasing the shell thickness could also enhance its pressure resistance. So, the hydrostatic pressure resistance of the proposed hydrophone could reach a high level as long as the shell is solid enough. It should be noted that the changes on the shell material and thickness would not affect the resonance characteristics of the cavity in the shell, because the resonance characteristics of the cavity are only related to the cavity size and sound speed [29].

2.4. Fabrication of the multi-resonance-cavity hydrophone

The composition of the eight-layer spherical cavity hydrophone is illustrated in Fig. 4. The hydrophone comprises two half shells made of photosensitive resin, manufactured via 3D printing, and a sensor circuit board. The shells feature several precisely designed grooves for securing the circuit boards. Eight micro-electromechanical system analog silicon microphones, model SPV0842LR5H, are utilized as the acoustic sensors due to their compact size, low power consumption, high sensitivity, and cost-effectiveness. Initially, the sensor circuit boards are embedded into the grooves of the half shells, aligning the microphones at the center of each cavity. Subsequently, the ultraviolet-curable adhesive is applied to bond and seal the two half shells. Each cavity serves as an output channel, sequentially numbered from 1 to 8 in order of the cavity size.

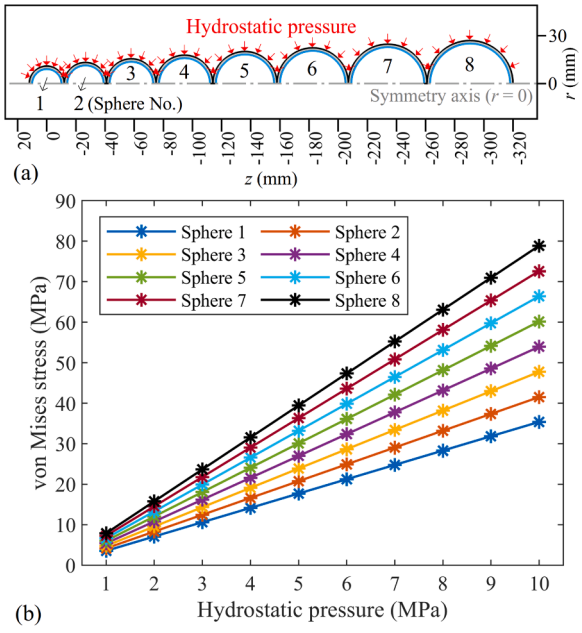

Fig. 3. Simulation on the hydrostatic pressure resistance of the hydrophone shell: (a) simulation model; (b) average von Mises stresses on the internal wall of each cavity.

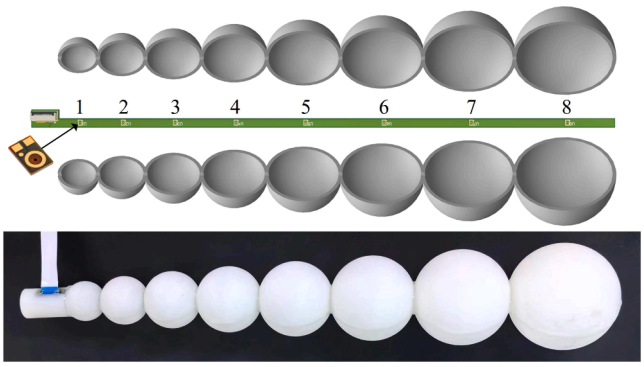

Fig. 4. Composition of the hydrophone.

3. Performance tests of the hydrophone

3.1. Testing system setup

A testing system for the multi-resonance-cavity hydrophone was set up in a glass water tank measuring 1.5 m × 1.5 m × 1.5 m in the laboratory, as illustrated in Fig. 5. The hydrophone was securely fastened to the linear guide at the top of the tank using a chuck and a rotary table, whilst the underwater transducer was hung at the same depth and 0.3 m away from the hydrophone. A piece of digital signal generated by the host computer was transmitted into the water via the transducer after being converted into analog signals by the data acquisition (DAQ) card and amplified by the power amplifier. Upon receiving the acoustic

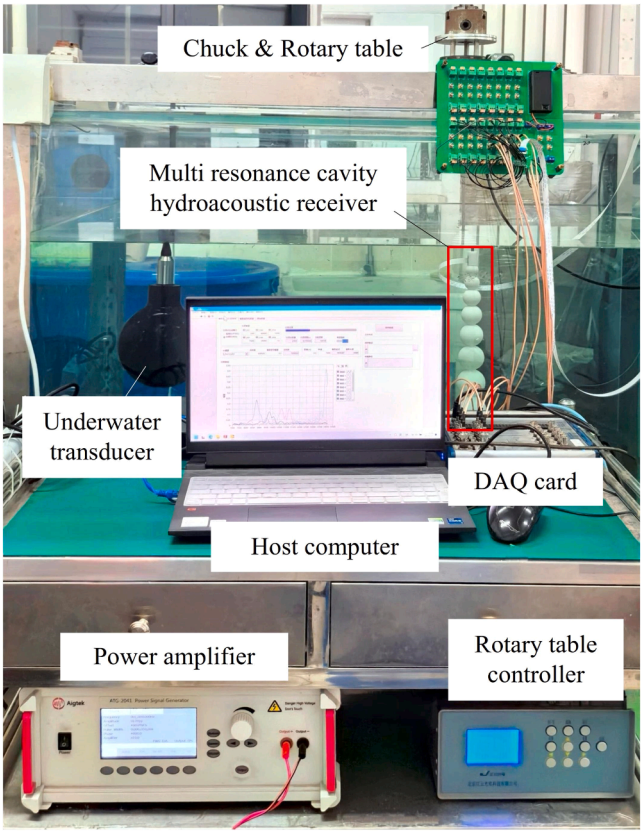

Fig. 5. Components of the hydrophone testing system.

signals, the hydrophone output multiple channels of analog signals, which were acquired by the DAQ card and transmitted to the host computer for data analysis. Additionally, the host computer could order the controller to rotate the rotary table. The DAQ card used is NI USB-6366, with the sample rate set to 500 kSps. The power amplifier model is Aigtek ATG-2041, and the underwater transducer model is ST-150.

With this testing system, a frequency sweep experiment was initially performed by gradually increasing the transmission signal frequency to evaluate the hydrophone's frequency response. The transmission frequency was then fixed at the third-order resonance frequency of the cavity, and the rotary table rotated a complete revolution to enable signal acquisition from multiple angles, evaluating the hydrophone's directivity. Subsequently, pulses at the resonance frequency of the cavity were emitted to evaluate the hydrophone's capability for single-frequency pulse reception.

3.2. Frequency response and directivity tests

Frequency response test was carried out within the frequency range of 7–27 kHz. The frequency response curves of each channel are illustrated in Fig. 6(a), where the resonance peaks corresponding to the third-order resonance frequency of each cavity are marked with colored arrows. The theoretical and experimental values of the third-order resonance frequencies are listed in Table I. The results indicate that each channel exhibits significantly high amplitudes at the resonance frequency. Although there is a slight deviation compared to the theoretical values for the third-order resonance frequency, it does not affect the normal usage of the hydrophone.

The directivity curves of each channel of the hydrophone at the third-order resonance frequency were tested separately, as shown in Fig. 6(b). The test results indicate that the directivity curves of each channel exhibit a circular or nearly circular shape at the third-order resonance frequency, indicating its omnidirectionality, which is consistent with the theoretical results.

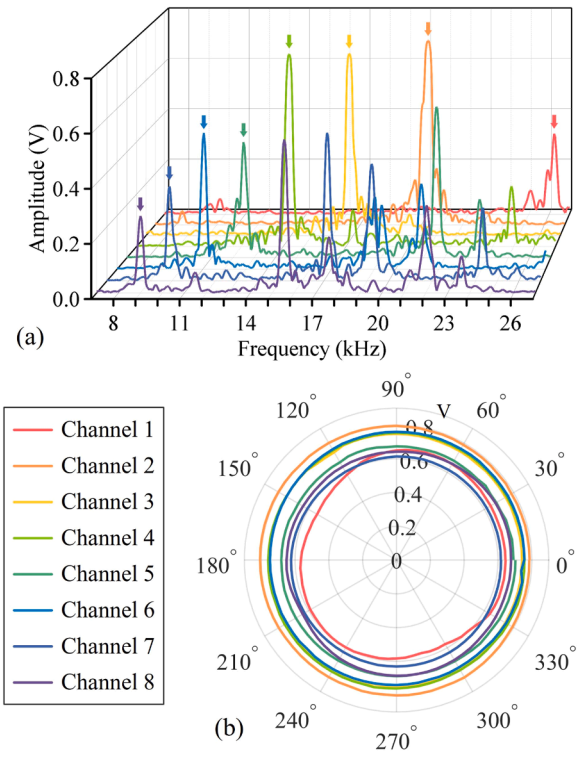

Fig. 6. Test results: (a) frequency response curves and (b) directivity curves of each channel of the hydrophone.

Table I
Theoretical and experimental values of the third-order resonance frequencies.

Channel No.	Radius (mm)	Resonance frequency (Hz)		Difference
		Theoretical	Experimental	
1	10	24544	26250	6.95 %
2	12.5	19635	20350	3.64 %
3	15	16363	16800	2.67 %
4	17.5	14025	14300	1.96 %
5	20	12272	12500	1.86 %
6	22.5	10908	11050	1.30 %
7	25	9817	9900	0.85 %
8	27.5	8925	9000	0.84 %

3.3. Single-frequency pulse receiving tests

Eight sets of experiments were conducted, sequentially emitting single-frequency pulses at the third-order resonance frequency of each cavity of the eight-cavity hydrophone into the water, with a total of 100 pulses per set. The time-domain waveforms for each channel of the hydrophone at the third-order resonance frequency of Cavity 2 are demonstrated in Fig. 7(a). From the time-domain waveform, it is evident that when the transducer emits pulses at this frequency, strong resonance occurs in Cavity 2, leading to a much higher amplitude of Channel 2 than the other channels. The pulse spectra of eight channels of the hydrophone obtained from each experiment set are shown in Fig. 7(b). It is obvious that each channel exhibits prominent resonance peaks when receiving the pulses at the third-order resonance frequency of the respective cavity, with relatively low amplitudes at other frequencies. Each channel is capable of effectively receiving pulse signals at the corresponding frequency.

4. Data transmission tests of the hydrophone

4.1. Data transmission method

The American Standard Code for Information Interchange (ASCII) is a character encoding scheme that maps a set of numbers to characters. The standard ASCII uses a 7-bit number to represent 128 characters, including the English alphabet (both uppercase and lowercase), numerals, and a variety of punctuation symbols. The extended ASCII uses an additional 8th bit on top of the standard ASCII to represent more characters, expanding the character set to accommodate 256 distinct characters. The proposed multi-resonance-cavity hydrophone has 8 channels, capable of simultaneously transmitting 8-bit binary numbers. Therefore, ASCII encoding can be employed to convert the data into a receivable format for the hydrophone.

A data transmission method with the proposed hydrophone is designed and its schematic diagram is illustrated in Fig. 8. The transmitted data is first encoded into decimal numbers ranging from 0 to 255 using ASCII encoding, which are then converted into 8-bit binary numbers. Based on the relationship between the binary numbers and the eight resonance frequencies, a mixed-frequency waveform is generated and transmitted into the water through the transducer, and then acquired by the hydrophone. The spectrum of the received signal is analyzed and the existences of eight frequency components are verified to derive the 8-bit binary numbers. These binary numbers are subsequently converted back into decimal numbers ranging from 0 to 255, and the data are finally decoded.

4.2. Generating and decoding the transmission signal

The steps for generating the transmission signal include encoding, mixing, and concatenating. In the host computer, a character to be transmitted is encoded into a decimal number ranging from 0 to 255 using ASCII, and then converted into an eight-bit binary number. Each bit of the binary number associates with each cavity of the multi-

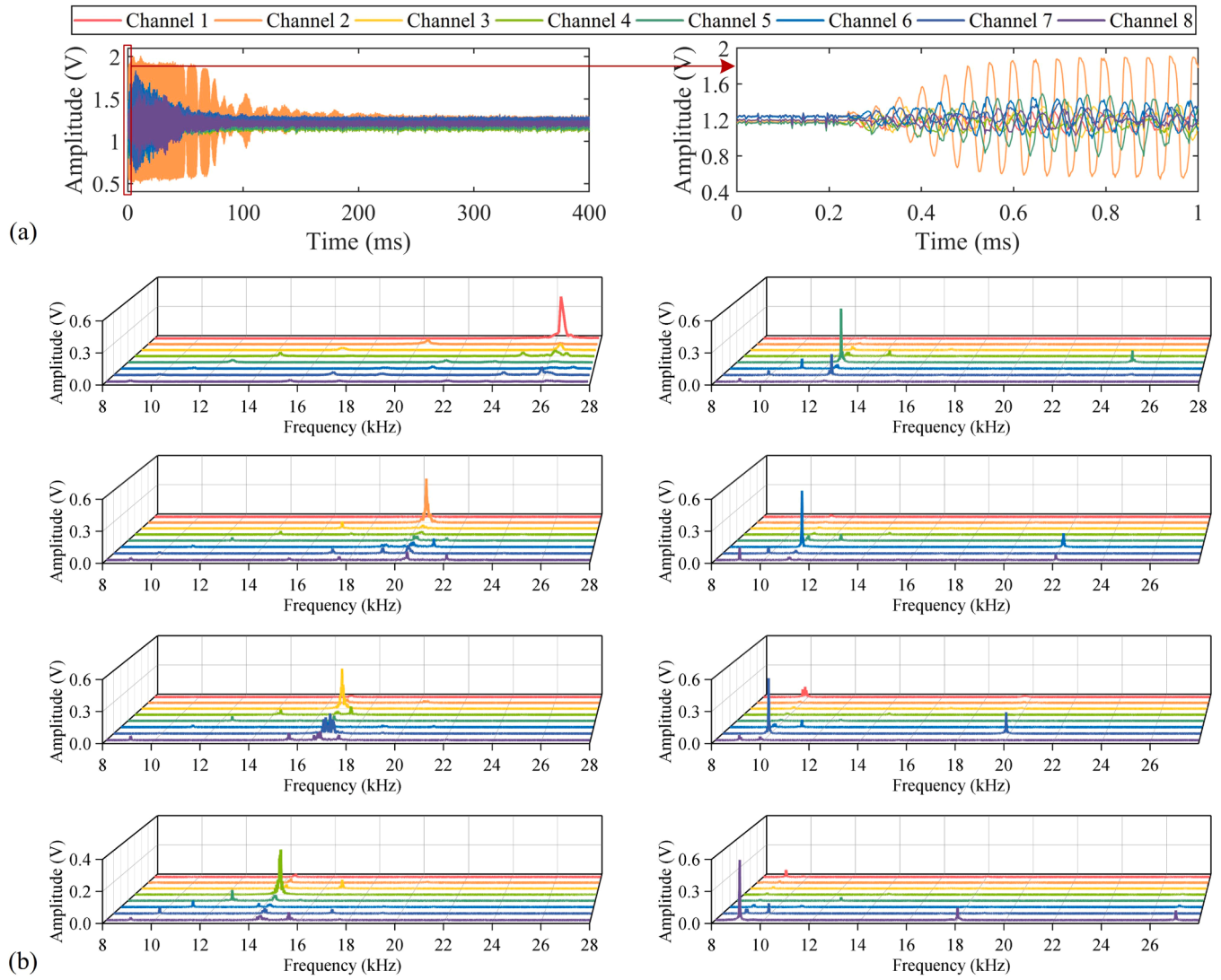

Fig. 7. Time-domain waveforms and frequency spectra of the single-frequency pulses received by the eight-cavity hydrophone: (a) the overall and local waveforms received by each channel at the third-order resonance frequency of Cavity 2; (b) the pulse spectra received by each channel in each experiment set.

resonance-cavity hydrophone. If a certain bit of the binary data is "1", a piece of fixed-length single-frequency pulse is mixed into the transmission signal of that character; if it is "0", no pulse is mixed in. All characters to be transmitted are converted into multiple segments of mixed-frequency signals, which are then concatenated together, with a certain interval left between each two segments.

The multi-resonance-cavity hydrophone captures acoustic signals and outputs analog voltage signals. The voltage signals are acquired by the DAQ card and uploaded to the host computer. The signal processing software on the host computer calculates the amplitudes of each third-order resonance frequency in real-time and compares them with the predefined thresholds. If the amplitude exceeds the threshold, indicating the presence of the corresponding frequency component in the transmitted signal, that bit of the binary number will be set to "1"; conversely, if the amplitude is below the threshold, indicating the absence of the frequency component, that bit of the binary number will be set to "0". After parsing the signals from all channels into binary numbers, they are converted into decimal numbers and then decoded into strings according to ASCII. During this process, the threshold for the signal amplitude needs to be predetermined. In this design, the threshold for each channel is set at 40 % of the amplitude when the binary "1" is received in that channel.

4.3. *Continuous transmission test*

If the multi-resonance-cavity hydrophone received numbers ranging from 0 to 255 successfully, data transmissions using ASCII would be feasible. Therefore, a continuous transmission test was conducted in an open-air lake, and a batch of numbers from 0 to 255 was used for transmission test. Additionally, the baud rate was measured during the test. When generating transmission signals, the duration of a single character signal was set to 5 ms, with an interval of 50 ms between two characters. The total length of the transmission signal was 14.08 s. The generated waveform of the transmission signal is illustrated in Fig. 9(a).

The complete time-domain waveforms received by each channel of the hydrophone are shown in Fig. 9(b), and Fig. 9(c) illustrates the time-domain waveforms and spectra of 85 (binary 01010101) and 170 (binary 10101010) received by each channel, with the corresponding binary numbers marked on the spectra. From the time-domain waveforms and spectra of the two sets of data, it can be observed that the channels receiving binary "1" have higher amplitudes and exhibit prominent resonance peaks at the corresponding frequencies; conversely, the channels receiving binary "0" have amplitudes close to zero, with either no resonance peaks or significantly lower resonance peak amplitudes. After analyzing the entire received data, it can be concluded that the 256 numbers were all accurately received and decoded with no error.

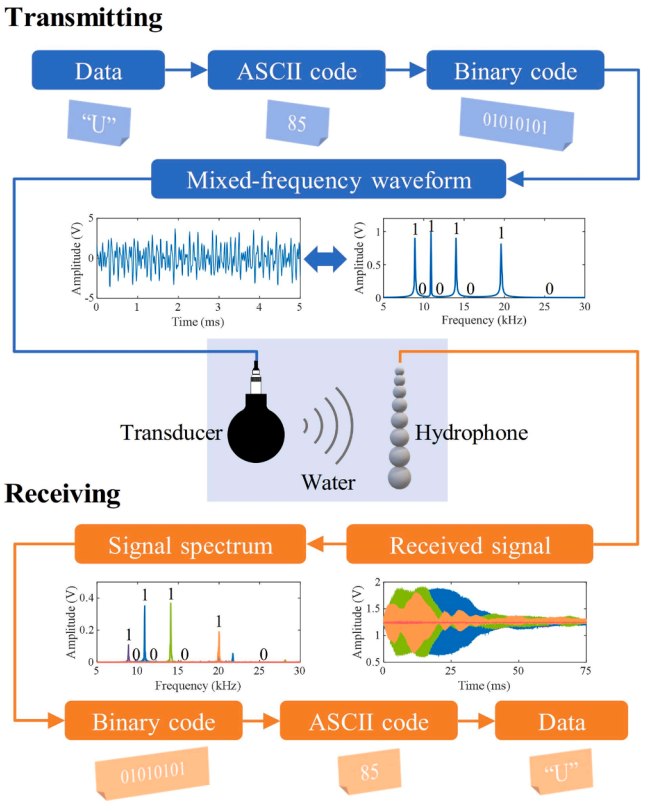

Fig. 8. Schematic diagram of data transmission technique with the hydrophone.

The test transmitted 256 numbers ranging from 0 to 255, since each number consists of 8 bits, the total data size is 2048 bits. The time to transmit a single number is 5 ms, with a 50 ms interval between two numbers, so the total transmission time is 14.08 s. Therefore, the baud rate equals 2048/14.08 ≈ 145.45 bps.

5. Conclusion

A multi-resonance-cavity hydrophone for underwater acoustic data transmission is proposed, which is composed of multiple resonant air cavities with shells and a sensor circuit board, enabling simultaneous reception of multiple bits of data. The acoustic resonance mechanism of rigid-wall spherical cavities is analyzed, and its resonance modes and directivity are clarified through finite element simulations. At the third-order resonance mode, the cavity center exhibits the highest absolute acoustic pressure and is omnidirectional, suitable for receiving acoustic signals from any direction. Theoretical analysis and parametric sweep simulations demonstrate the inversely proportional relationship between the resonance frequency and the radius, allowing precise tuning of the resonance frequency by adjusting the cavity radius.

An eight-layer spherical cavity hydrophone is designed, and its frequency response is simulated, which proves that the center of each cavity exhibits prominent absolute acoustic pressure at their resonance frequencies, and the presence of the shell and sensor circuit board has minimal effect on the resonance mode of the cavity. The hydrostatic pressure resistance of the proposed hydrophone shell is simulated, and it can be inferred that the 2 mm thick photosensitive resin shell can theoretically resist the hydrostatic pressure of about 7 MPa. The fabrication of the hydrophone is introduced, and a testing system for the hydrophone is set up in the laboratory. The hydrophone is verified to function properly through frequency sweep tests. The resonance peak positions in the frequency response curves are almost consistent with the theoretical and simulation results. Directivity tests confirm that each

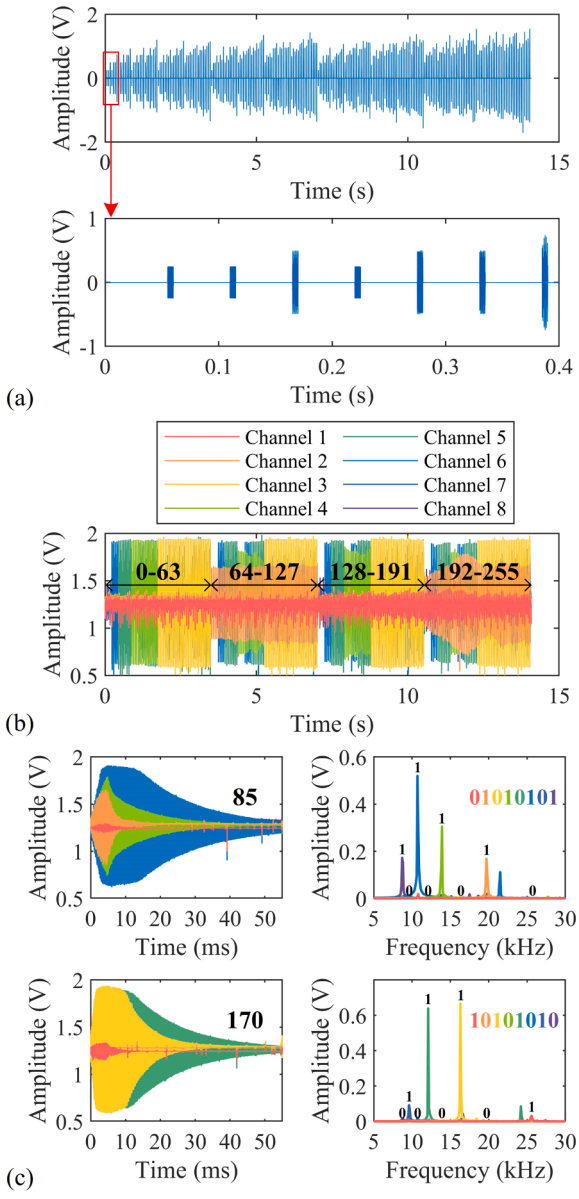

Fig. 9. Data transmission test of the proposed hydrophone: (a) waveform of the transmission signal; (b) complete time-domain waveforms received by each channel; (c) time-domain waveforms and spectra of the received numbers 85 and 170.

channel exhibited omnidirectionality at their third-order resonance frequencies. Single-frequency pulse receiving tests demonstrate that each channel can effectively receive pulse signals at the corresponding frequency.

A data transmission method with the proposed hydrophone is designed, along with the process of generating and decoding transmission signals. The performance of underwater data transmission is tested by transmitting a batch of numbers from 0 to 255 in the lake. The test results indicate that the multi-resonance-cavity hydrophone can accurately receive all data at the baud rate of 145.45 bps with no error.

CRediT authorship contribution statement

Jinyu Ma: Writing – review & editing, Supervision. **Xinjing Huang:** Writing – review & editing, Supervision, Funding acquisition, Conceptualization. **Zan Li:** Writing – original draft, Validation, Data curation. **Tian Yang:** Investigation, Data curation. **Jian Li:** Project

administration.

Declaration of Competing Interest

The authors declare that they have no known competing financial interests or personal relationships that could have appeared to influence the work reported in this paper

Acknowledgements

This work is supported by National Natural Science Foundation of China (Nos. 62073233, 62473279) and Guangxi Key Laboratory of Automatic Detecting Technology and Instruments (No. YQ24203).

Data Availability

The authors do not have permission to share data.

References

[1] N. Hua, X. Chen, P. Chen, W. Song, W. He, Stereoscopic perception system for marine environment monitoring, China Offshore Platf. 36 (01) (2021) 78–83, https://doi.org/10.12226/j.issn.1001-4500.2021.01.20200614.
[2] C. Zhong, J. Lu, D. Kang, Q. Liang, Design of a multiparameter data acquisition and control system for in situ seabed observation base stations, IET Sci. Meas. Technol. 18 (1) (2024) 33–47, https://doi.org/10.1049/smt2.12169.
[3] S. Sun, Seabed-base marine environment automatic monitoring system, Ocean Technol. 19 (04) (2000) 1–7.
[4] S. Sun, The development and application of automatic seabed-based monitoring platform technology, Ocean Technol. 22 (03) (2003) 81–84.
[5] F. Yu, Y. Chen, C. Zhou, X. Zhang, K. Deng, Y. Han, et al., Design of deep-sea quasi-real-time-communication submerged buoy systems, Mar. Sci. 44 (07) (2020) 194–200, https://doi.org/10.11759/hykx20200327004.
[6] T. Kanazawa, Japan Trench earthquake and tsunami monitoring network of cable-linked 150 ocean bottom observatories and its impact to earth disaster science, 2013 IEEE Int. Underw. Technol. Symp. (2013) 1–5, https://doi.org/10.1109/UT.2013.6519911.
[7] R. Dewey, A. Round, P. Macoun, J. Vervynck, V. Tunnicliffe, The VENUS cabled observatory: engineering meets science on the seafloor, Oceans 2007 (2007), https://doi.org/10.1109/OCEANS.2007.4449171.
[8] S. Taylor, Transformative ocean science through the VENUS and NEPTUNE Canada ocean observing systems, Nucl. Instrum. Methods Phys. Res. A 602 (2009) 63–67, https://doi.org/10.1016/j.nima.2008.12.019.
[9] J. Chen, D. Zhang, X. Wang, X. Pan, C. Wang, Z. Zhang, et al., Research on the state-of-the-art and trends of seafloor observatory, J. Ocean Technol. 38 (06) (2019) 95–103, https://doi.org/10.3969/j.issn.1003-2029.2019.06.015.
[10] P. Li, X. Han, W. Nie, C. Chang, G. Li, P. Liao, et al., The research progress in underwater wireless optical communication technology, First Int. Conf. Spat. Atmos. Mar. Environ. Opt. 127060T (2023), https://doi.org/10.1117/12.2682867.
[11] B. Wang, Q. Wu, L. Liu, T. Wang, R. Zhu, P. Zhang, et al., Research progress on the underwater wireless optical communication system, Laser Technol. 46 (01) (2022) 99–109, https://doi.org/10.7510/jgjs.issn.1001-3806.2022.01.010.
[12] A.A. Abdou, An Investigation of Short Range Electromagnetic Wave Communication for Underwater Environmental Monitoring Utilising a Sensor Network Platform, Liverpool John Moores University, United Kingdom, 2014.
[13] J. Farmer, R. Moorhead, B. Tang, R. Green, J. Moorhead, Underwater wireless electromagnetic/radio communication using software defined radios, OCEANS 2022 (2022) 1–7, https://doi.org/10.1109/OCEANS47191.2022.9977153.
[14] M. Chitre, S. Shahabudeen, M. Stojanovic, Underwater acoustic communications and networking: Recent advances and future challenges, Mar. Technol. Soc. J. 42 (1) (2008) 103–116, https://doi.org/10.4031/002533208786861263.
[15] J. Yang, J. Wang, G. Qiao, S. Liu, L. Ma, P. He, Review of underwater acoustic communication and network technology, J. Electron. Inf. Technol. 46 (01) (2024) 1–21, https://doi.org/10.11999/JEIT230424.
[16] W. Shi, C. He, Q. Dang, L. Jing, Single-carrier with index modulation for underwater acoustic communications, Appl. Acoust. 172 (2021) 107572, https://doi.org/10.1016/j.apacoust.2020.107572.
[17] H. Khelladi, M.A. Mograne, Optimization of some acoustic parameters intended for the wireless communication in seawater, Appl. Acoust. 154 (2019) 59–67, https://doi.org/10.1016/j.apacoust.2019.04.020.
[18] R. Chen, W. Wu, Q. Zeng, S. Liu, Construction and application of polar codes in OFDM underwater acoustic communication, Appl. Acoust. 211 (2023) 109473, https://doi.org/10.1016/j.apacoust.2023.109473.
[19] O.M. Bushnaq, I.V. Zhilin, G.D. Masi, E. Natalizio, I.F. Akyildiz, Automatic network slicing for admission control, routing, and resource allocation in underwater acoustic communication systems, IEEE Access 10 (2022) 134440–134454, https://doi.org/10.1109/ACCESS.2022.3231607.
[20] N. Motsi, G. Stamou, S. Angelopoulos, A. Ktena, E. Hristoforou, Development of a high sensitivity hydrophone at a spectrum range from 0.1 Hz to 100 kHz, Sens. Actuators A: Phys. 372 (2024), https://doi.org/10.1016/j.sna.2024.115338.
[21] S. Wang, Y. Wang, Z. Wang, Z. Wu, Y. Xin, X. Zhou, A brief review on hydrophone based on PVDF piezoelectric film, Ferroelectrics 603 (2023) 150–156, https://doi.org/10.1080/00150193.2022.2159227.
[22] H. Saheban, Z. Kordrostami, Hydrophones, fundamental features, design considerations, and various structures: a review, Sens. Actuators A: Phys. 329 (2021) 112790, https://doi.org/10.1016/j.sna.2021.112790.
[23] S. Shi, W. Geng, K. Bi, J. He, X. Hou, J. Mu, et al., Design and fabrication of a novel MEMS piezoelectric hydrophone, Sens. Actuators, A: Phys. 313 (2020), https://doi.org/10.1016/j.sna.2020.112203.
[24] C. Lyu, S. Zhang, G. Fang, J. Jie, X. Zhang, C. Wu, Performance of dual-frequency ultrasound measurement based on DBR fiber laser hydrophone, Sens. Actuators, A: Phys. 266 (2017) 101–110, https://doi.org/10.1016/j.sna.2017.09.017.
[25] A. Cutolo, R. Bernini, G.M. Berruti, G. Breglio, F.A. Bruno, S. Buontempo, et al., Innovative photonic sensors for safety and security, part II: aerospace and submarine applications, Sensors (Basel) 23 (5) (2023), https://doi.org/10.3390/s23052417.
[26] S. Guardato, R. Riccio, M. Janneh, F.A. Bruno, M. Pisco, A. Cusano, et al., An innovative fiber-optic hydrophone for seismology: testing detection capacity for very low-energy earthquakes, Sensors (Basel) 23 (7) (2023), https://doi.org/10.3390/s23073374.
[27] M. Janneh, F.A. Bruno, S. Guardato, G.P. Donnarumma, G. Iannaccone, G. Gruca, et al., Field demonstration of an optical fiber hydrophone for seismic monitoring at Campi-Flegrei caldera, Opt. Laser Technol. 158 (2023) 108920, https://doi.org/10.1016/j.optlastec.2022.108920.
[28] F.A. Bruno, M. Janneh, A. Gunda, R. Kyselica, P. Stajanca, S. Werzinger, et al., Fiber optic hydrophones for towed array applications, Opt. Lasers Eng. 160 (2023) 107269, https://doi.org/10.1016/j.optlaseng.2022.107269.
[29] X. Huang, Z. Li, J. Li, X. Wang, H. Feng, Y. Zhang, et al., Low-cost, high-sensitivity hydrophone based on resonant air cavity, IEEE Sens. J. 21 (6) (2021) 7348–7357, https://doi.org/10.1109/JSEN.2020.3048066.
[30] X. Huang, Z. Li, J. Li, H. Feng, Y. Zhang, S. Chen, Acoustic investigation of high-sensitivity spherical leak detector for liquid-filled pipelines, Appl. Acoust. 174 (2021) 107790, https://doi.org/10.1016/j.apacoust.2020.107790.
[31] J. Cheng, Principles of Acoustics, Science Press, Beijing, 2012, pp. 411–439.

Li Zan received his B.E. and M.E. degrees both in Instrument Science and Technology from Tianjin University, Tianjin, China, in 2019 and 2022, respectively. He is currently working toward the Ph.D. degree with the State Key Laboratory of Precision Measurement Technology and Instruments, Tianjin University. His research interests include underwater acoustic sensing and acoustic metamaterials.

Yang Tian received her B.E. degree in Instrument Science and Technology from Shandong University, Jinan, China, in 2021. She received her M.E. degree in Instrument Science and Technology from Tianjin University, Tianjin, China, in 2024. Her research interests include underwater acoustic sensing.

Li Jian received his B.E., M.E., and Ph.D. degrees in Instrument Science and Technology from Tianjin University, Tianjin, China, in 1994, 1997, and 2000, respectively. He is currently a full professor in School of Precision Instrument and Opto-Electronics Engineering at Tianjin University. He also works at State Key Laboratory of Precision Measurement Technology and Instruments, Tianjin University. His research topics mainly cover test signal processing, weak signal detection, and target detection technology and instruments.

Ma Jinyu received her B.E. and M.E. degrees both in Instrument Science and Technology from Shandong University of Science and Technology, Qingdao, China, in 2010 and 2012, respectively. She received her Ph.D. degree in Instrument Science and Technology from Tianjin University, Tianjin, China, in 2016. In 2016, she joined the Sensor and Electronic Testing Laboratory of Tianjin University as a lecturer and engineer. She also works at State Key Laboratory of Precision Measurement Technology and Instruments, Tianjin University. Her research topics mainly cover electric sensing and measurement, precision measuring circuit, measurement and control based on embedded system.

Huang Xinjing received his B.Sc. and Ph.D. degrees both in Instrument Science and Technology from Tianjin University, Tianjin, China, in 2010 and 2016, respectively. In 2016, he joined the Modern Acoustic Testing Laboratory of Tianjin University as an assistant professor. Since 2020, He has been an associate professor in the School of Precision Instrument and Opto-Electronics Engineering at Tianjin University. He also works at State Key Laboratory of Precision Measurement Technology and Instruments, Tianjin University. His research topics mainly cover structural health inspection and/or monitoring technology, acoustic metamaterial device and sensor, magnetic/acoustic sensing and measurement, intelligent perception electronic system.